Chapter 3

Probing Giant Magnetism on Fe-N Thin Film by Polarized Neutron Reflectivity

Xiaowei Zhang, Nian Ji, Valeria Lauter, Haile Ambaye and Jian-Ping Wang

Additional information is available at the end of the chapter

http://dx.doi.org/10.5772/62726

Abstract

With the development in hard drive and permanent magnet industry, higher saturation magnetization (Ms) or magnetic induction (Bs) material is on high demand. According to the Slater-Pauling curve, the highest Bs value is ~2.45 T, which belongs to FeCo alloy. However, in 1972, Kim and Takahashi [1] announced that the new material Fe-N thin film exhibited an increase in the Bs value of 18%. From then on, tons of research works [2, 3, 4] had been dedicated in this area with conclusions on both sides, achieving either high Bs or low Bs. Among those works, the Bs values were obtained from the measurement of the thin film magnetic moment and its volume, which might cause a considerable amount of error depending on the accuracy of the film thickness and area measurement. Other concerns also include the uncertainty of Ms value due to the subtraction of Fe underlayer. Indeed, a direct measurement of Bs is the key to clarify the discrepancies between these results. Here, we are presenting the method of polarized neutron reflectometry (PNR) to measure the Bs of the partially ordered $Fe_{16}N_2$ thin film. PNR allows the interface magnetism study, [5] the *absolute* magnetization determination and magnetic depth profile in single thin films, [6, 7, 8, 9] and complicated superlattice structures. [10, 11] In the following scenarios, different partially ordered $Fe_{16}N_2$ thin films are fabricated and are measured using PNR subsequently. Their Bs values are obtained using the fitting results of nuclear scattering length density (NSLD) and magnetic scattering length density (MSLD). Also, a PNR application on FeN thin film will also help us to understand the switching picture of the FeN thin film with external applied field.

Keywords: $Fe_{16}N_2$, high saturation magnetization, polarized neutron reflectivity, thin film

1. Introduction

1.1. PNR Introduction

The interaction of neutrons with matter can be described in the optical formalism using the concept of reflective index for the medium. This can be obtained by Schrödinger equation, where the interaction of the neutron with medium is denoted by V:

$$\left[-\frac{\hbar^2}{2m}(\Delta + k_0^2) + V\right]\Psi = 0 \tag{1}$$

$$\frac{\hbar k_0^2}{2m} = \omega \tag{2}$$

where m is the neutron mass, k_0 is the wave vector in vacuum, $\hbar\omega$ is its energy. So the refractive index can be written as:

$$n^2 = 1 - V / \hbar\omega \tag{3}$$

Here, we can define the strong interaction potential with born approximation, which can be described by the Fermi pseudopotential: [12]

$$V_F(r) = b\left(\frac{2\pi\hbar^2}{m}\right)\delta(r), \tag{4}$$

where b is the scattering length and r is neutron position. The mean potential of the interaction between neutron and medium is the given by the integration of the space:

$$V = \frac{1}{V}\int V(r)d^3r = \frac{2\pi\hbar^2}{m}Nb, \tag{5}$$

where N denotes the number density of the atoms. The multiplicity of number density and scattering length is called scattering length density (SLD) ρ.

2. Specular reflectivity of neutrons from interface

If we compare the situation of neutron reflection to the light propagation at the interface of different mediums, the different interaction potential of neutron with medium can be seen as different mediums with different refraction indices. This follows Fresnel equations (Fig. 1).

http://dx.doi.org/10.5772/62726

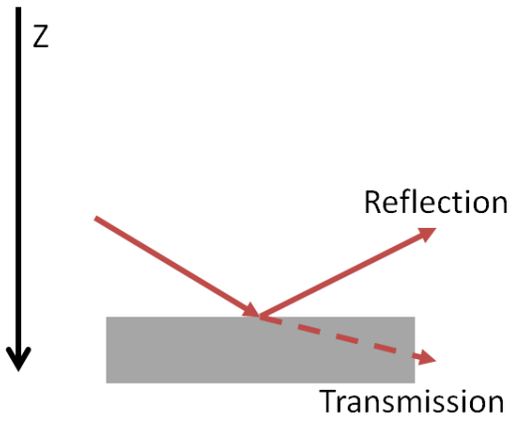

Figure 1. A schematic illustration of neutron interacting with matters at the interface obeys the Fresnel equations in analogy to the optical formalism.

$$R = |r|^2 = \left| \frac{k_1 - k_2}{k_1 + k_2} e^{i2k_1 z} \right|^2$$
$$T = |t|^2 = \left| \frac{2k_1}{k_1 + k_2} e^{i2(k_1 - k_2)z} \right|^2 \quad (6)$$

For bulk materials, after applying Snell-Descartes' law, the reflection coefficient at a small incident angle can be written as a function of the wave-vector transfer q:

$$R(q) = \left| \frac{q_z - \sqrt{q_z^2 - q_c^2}}{q_z + \sqrt{q_z^2 - q_c^2}} \right|^2, \quad (7)$$

where q_c is the wave vector, which corresponds to critical angle of total external reflection. It is also easy to show that at high q limit, the reflectivity R follows the $1/q^4$ power law (Fresnel decay).

Dynamic calculation can also be applied with Born approximation. The reflectivity is equal to the Fourier transformation of the SLD profile: [13]

$$R = \frac{1}{q_z^2} \left| \int_{-\infty}^{\infty} \mathrm{e}^{iq_z y} \rho(y) \mathrm{d}y \right|^2. \quad (8)$$

It is worth mentioning that Fresnel decay originates from a planar surface and the decay will result in a extremely low intensity at high q value, which will be very difficult to collect with the mixture of background noise or incoherent scattering from the substrate.

The critical angle θ_c is usually small and can be written as follows at the total reflection condition:

$$\cos\theta_c = n = 1 - \frac{\lambda^2}{2\pi} Nb, \tag{9}$$

where λ is the wavelength. It is useful to use Taylor expansion. Therefore, the critical angle θ_c and the corresponding critical wave vector q_c are

$$\theta_c = \sqrt{\frac{Nb}{\pi}}\lambda \tag{10}$$

$$q_c = 4\sqrt{\pi Nb}. \tag{11}$$

Usually the thickness of the thin film is larger than the wavelength of neutron, and so the reflecting beams of the neutron will give constructive/destructive patterns according to Bragg's diffraction law. Figure 2 is an example of a reflectivity from a bare bulk substrate and of a typical thin film:

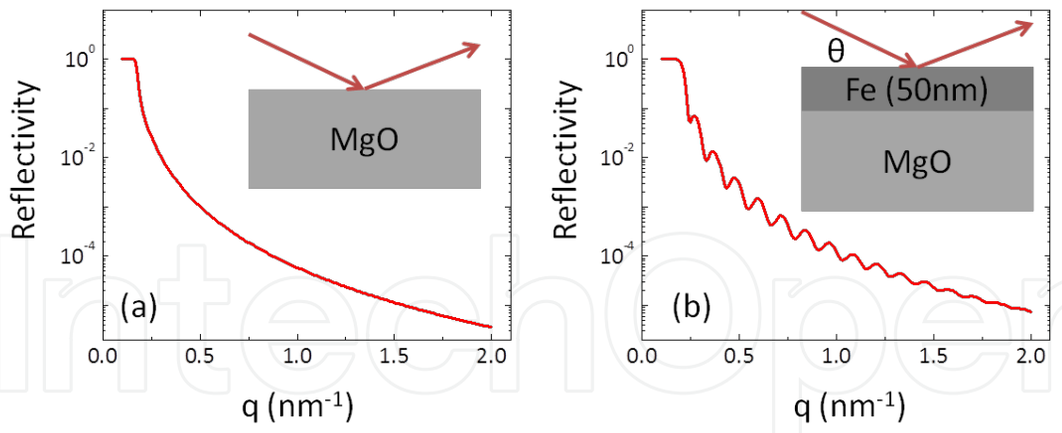

Figure 2. Simulated neutron reflectivity curves of (a) a flat MgO substrate and (b) a flat 50-nm-thick Fe thin film grown on MgO substrate.

3. Neutron reflectivity from a magnetic interface

In the presence of an external magnetic field, B, Zeeman energy will be present due to the spin of neutron itself:

http://dx.doi.org/10.5772/62726

$$V_Z = -g_n \mu_n B, \tag{12}$$

where $g_n \mu_n$ gives the neutron magnetic moment. Since $B = \mu_0 H + M$, where M is the magnetization of the material, we can express the potential in terms of M. At the magnetic interface with the addition of this energy, the total interaction potential energy between the neutron and medium can be written as follows:

$$V = \frac{2\pi\hbar^2}{m}(\rho_n \pm \rho_m), \tag{13}$$

where ρ_n is the nuclear SLD of the medium and ρ_m is the magnetic SLD of the medium, which can be defined by:

$$\rho_m = -\frac{m}{2\pi\hbar^2}\mu_n \sum M. \tag{14}$$

The sign ± represents spin-up and spin-down cases corresponding to the magnetization of the medium. In respect to neutron polarization, this shows that the magnetic SLD is directly related with the magnetization in the medium that the neutron is shining upon, which gives a direct measurement of the saturation magnetization when saturated in the external field.

Similarly, the critical angle θ_c and corresponding critical wave vector q_c can be written as:

$$\theta_c = \sqrt{\frac{\rho_n \pm \rho_m}{\pi}}\lambda \tag{15}$$

$$q_c = 4\sqrt{\pi(\rho_n \pm \rho_m)}. \tag{16}$$

Therefore, spin-up reflectivity will have a large critical angle/momentum transfer compared to spin-down reflectivity (Fig. 3). If we present the potential in the matrix form with Pauli operator, then:

$$V = \frac{2\pi\hbar^2}{m}\begin{pmatrix}\rho_n & 0\\ 0 & \rho_n\end{pmatrix} \mp \mu_n \begin{pmatrix}B_z & B_x - iB_y\\ B_x + iB_y & -B_z\end{pmatrix} = \frac{2\pi\hbar^2}{m}\begin{pmatrix}\rho_n + \rho_{mz} & \rho_{mx} - i\rho_{my}\\ \rho_{mx} - i\rho_{my} & \rho_n - \rho_{mz}\end{pmatrix}. \tag{17}$$

The potential we obtained above is the diagonal terms, which corresponds to the non-spin flip situation. The off diagonal terms [14]will represent the spin flip situation, which will not be discussed in this article.

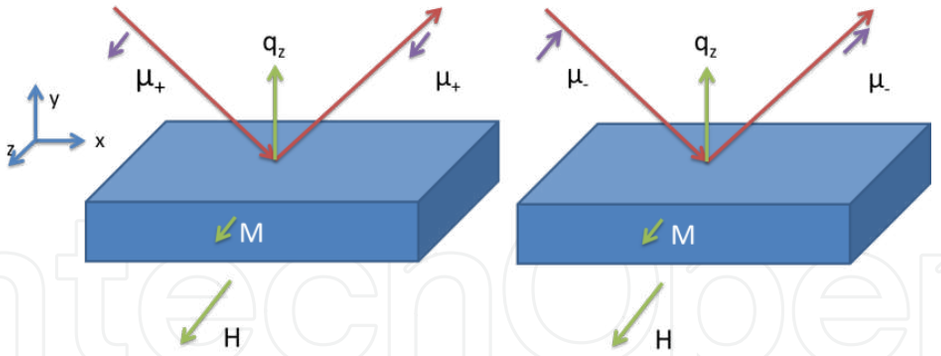

Figure 3. Polarized neutron reflectivity with two different spin polarizations. The spin-up (μ+) and spin-down (μ–) neutrons are indexed as parallel and anti-parallel with respect to the external field direction.

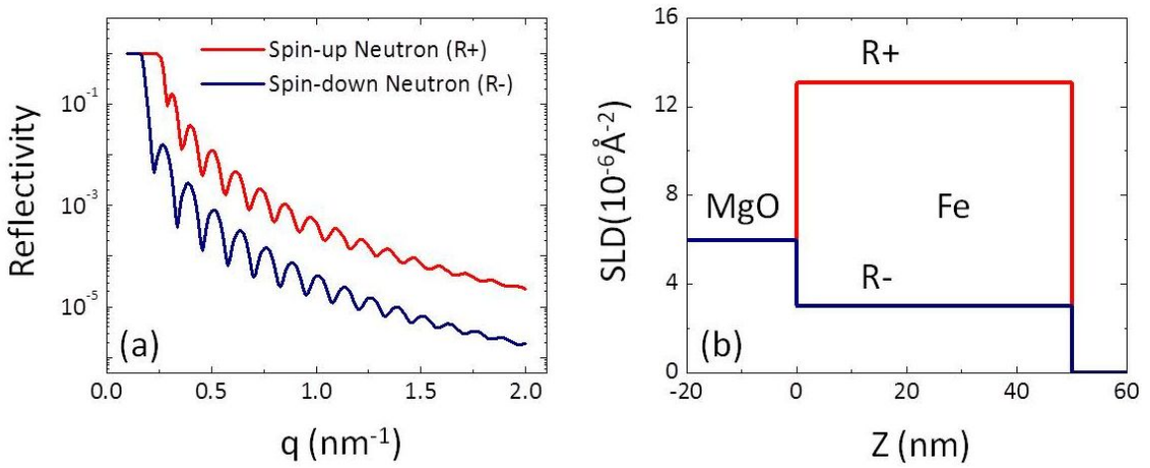

Figure 4. (a) The simulated reflectivities of a 50-nm Fe thin film grown on MgO substrate after saturation in-plane with external field. (b) The depth-dependent SLD according to the reflectivity curves in (a).

As seen from the reflectivity curves (Fig. 4), the magnetic interaction splits the non-magnetic oscillation curve into two branches. Fitting the reflectivity will yield the SLD for each spin case:

$$\begin{aligned} \rho_{tot+} &= \rho_n + \rho_m \\ \rho_{tot-} &= \rho_n - \rho_m . \end{aligned} \tag{18}$$

We can solve for ρ_m and, therefore, retrieve the Ms of the sample.

4. Giant Bs induced by strain effect on epitaxial $Fe_{16}N_2$ thin film [15]

Two sets of partially ordered $Fe_{16}N_2$ thin film samples are fabricated on MgO substrate with facing target sputtering system. After the deposition of Fe underlayer at 300°C, a Fe-N layer

http://dx.doi.org/10.5772/62726

is grown subsequently on the top of Fe layer at room temperature with the optimum volume ratio of N_2 and Ar mixture so that the stoichiometry in Fe-N layer is Fe/N=8:1. An in-situ annealing is carried out right after at 120°C for 20 hours in vacuum. To explore the in-plane tensile strain effect on the Bs value of Fe-N thin film, two samples are grown with different Fe underlayers, 2 nm and 20 nm, respectively.

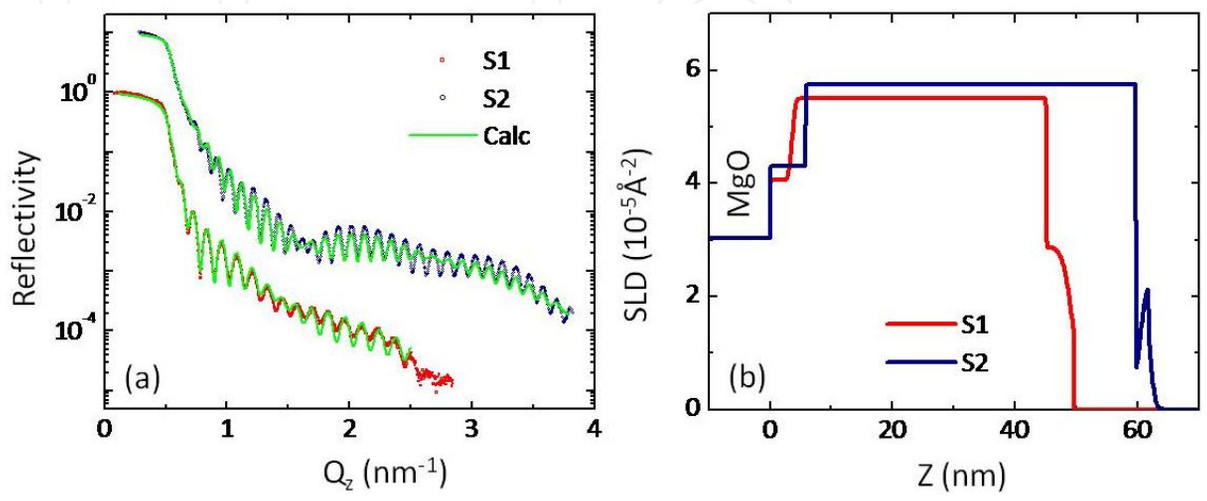

Figure 5. X-ray reflectivity characterization. (a) The fitted x-ray reflectivity curves measured on samples S1 and S2 (vertically offset by a factor of 10). (b) Calculated depth-dependent x-ray SLD profiles.

Both samples are investigated by PNR using the Magnetism Reflectometer at Spallation Neutron Source at Oak Ridge National Laboratory (SNS ORNL). [16] The reflectivities with the spin of the neutrons being either parallel (R^+) or anti-parallel (R^-) to the applied magnetic field are collected simultaneously. From these data the depth profiles of the SLD of both NSLD and MSLD are obtained. The PNR experiments are performed at room temperature in the saturation external field of H=1.0 T applied in-plane of the sample. The R^+ and R^- reflectivity data are fitted simultaneously using a genetic algorithm with an exact recursive matrix calculation embedded in the *Simulreflec 1.0* package. [17] The experimental reflectivity and calculated curves with best chi-squared fit for samples S1 and S2 are shown on Fig. 6a and b, respectively. Their corresponding structural NSLD and magnetization depth profiles are plotted in Fig. 6c and d.

In data modeling process, the structural NSLD and layer choice were constrained to closely match X-ray Reflectivity (XRR) results (Fig. 5). To account for the possibility that the film possess homogeneous chemical composition but potentially different magnetization, the Fe-N layer was subdivided into three slabs where NSLD are forced to be identical but thickness, roughness, and MSLD were allowed to vary independently. When fitting the data to extract the physical depth profile of the film structure, the only free parameter that was allowed to vary was the magnetization as other parameters were already framed by the XRR result and only marginal improvement was possible. After the comparison of the XRR and PNR result, we can find a relatively large roughness at high Q range, which is most likely due to either not

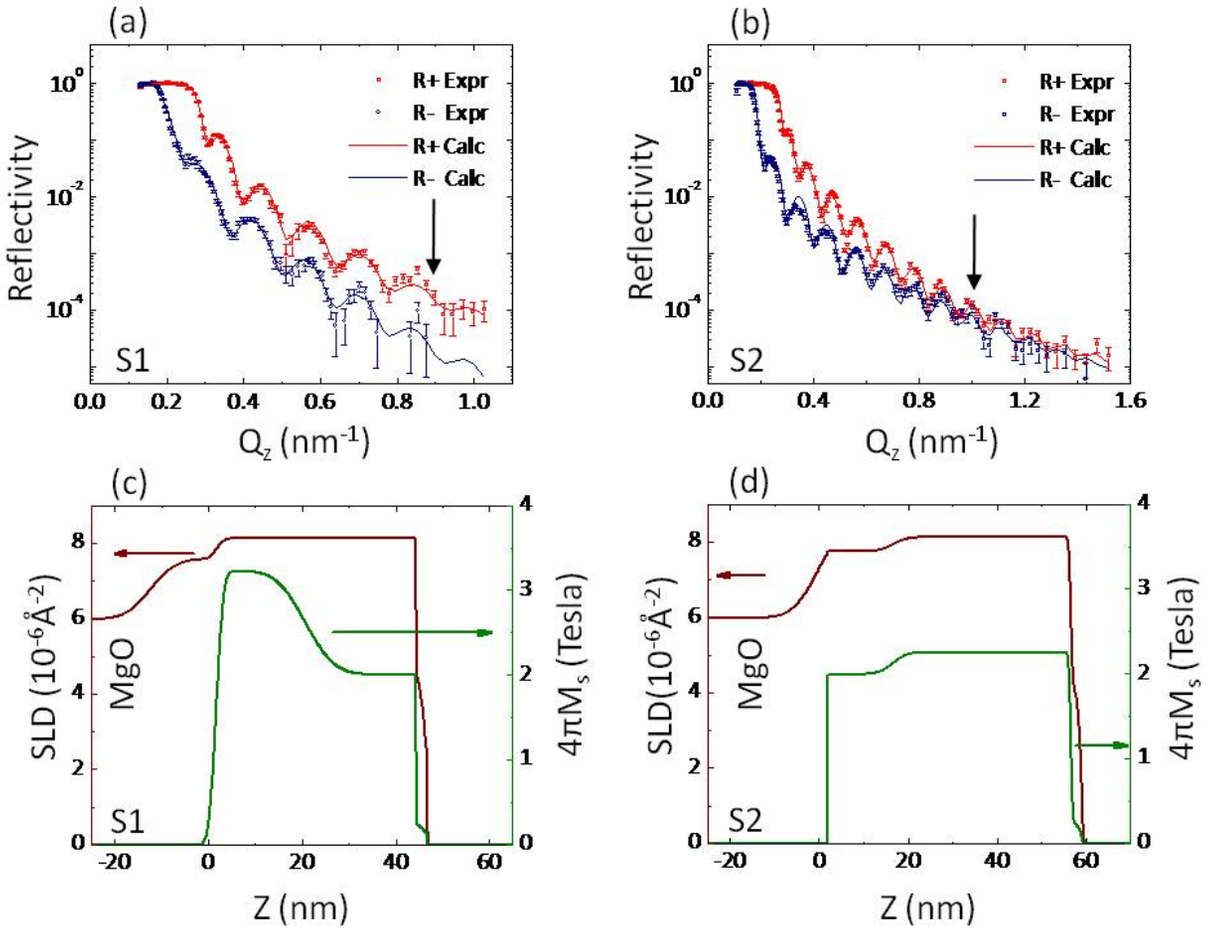

Figure 6. Polarized neutron reflectivity characterization. (a) and (b) Experimental polarized neutron reflectivities together with the fitted curves as functions of momentum transfer Q for samples S1 and S2 as labeled, respectively. The arrows at high Q region (>0.8nm^{-1}) indicate the difference of the magnetic properties toward the bottom interface between these two samples. (c) and (d) Structural (Brown) and magnetic (Green) depth profiles for samples S1 and S2 as labeled correspondingly.

enough data acquisition at this specific range or the chemical compound that is formed at the interface during the thin film growth or annealing process, such as MgO:N.

It is very obvious that an anomalously large magnetization is formed at the bottom of the film with a range of about 20 nm. The MSLD for this part of the film is 7.2~7.5 × 10^{-6}Å^{-2}, which in turn means the Ms value is 3.1~3.2 T. This value is significantly higher than bulk Fe (40~50%) and $Fe_{65}Co_{35}$ (20~30%). When the SLD profile extends to higher layer of the film, the MSLD values drops to 4.66 × 10^{-6}Å^{-2} and represents a low Ms value of 2.01 T. This non-uniformity of the magnetization across the film cannot be replaced by single layer model, which will fail to resemble the reflectivity behavior of the experiment. For sample S2, the resulted MSLD is close to 5 × 10^{-6}Å^{-2} for the Fe-N layer, corresponding to Ms of 2.15 T, which does not show the presence of giant Bs. The different Bs results of the two samples are due to the strain that is experienced by the epitaxial growth of the Fe-N layer. In sample S1, larger in-plane tensile strain contributes to high Bs.

http://dx.doi.org/10.5772/62726

Further justification for the different magnetic structure upon Fe buffer thickness change comes from the spin asymmetry (SA) $(R^+–R^-)/(R^++R^-)$ plot shown in Fig. 7. SA of both samples were fitted with experiment data. Initially, the SA values of both samples are oscillating at a high value. However, the SA value of sample S2 drops rapidly close to zero, whereas that of sample S1 almost reaches unity. In this high scattering vector region (q>0.8nm^{-1}), the interface of the bottom layer will dominate MSLD and NSLD. To account for the disparity of the different behaviors of two samples, |MSLD–NSLD| >> MSLD needs to be satisfied for sample S1. Since NSLD is similar for both samples, this observed feature directly proves the substantial enhancement of MSLD in the high Ms sample comparing to that of S2 at the bottom interface.

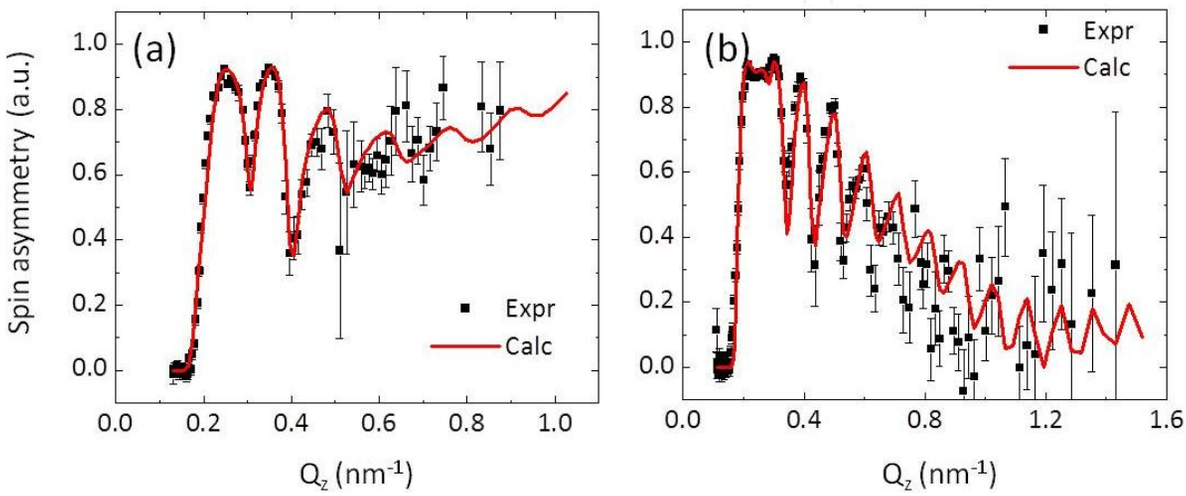

Figure 7. Spin asymmetry plotting of samples S1 (a) and S2 (b). It is clear as it approaches high q, the trend of the curves are different for these two samples.

5. High Bs obtained on partially ordered $Fe_{16}N_2$ multilayer thin film [16]

Multilayer structures are very common in many areas that they can bring many new physical phenomena. To explore the possibility of applying $Fe_{16}N_2$ in multilayer structure, two samples are fabricated on GaAs substrate with Fe/Fe-N layer stack. Samples L1 and L3 are with 1 and 3 repetitions, respectively.

It is known that co-refining the x-ray and neutron reflectivity curves allows an unambiguous determination of magnetic depth profile. [19, 20] When modeling the chemical part of the film structure, consistent structure for fitting both samples is set the same for both PNR and XRR. In this case, only marginal adjustment is allowed during the fitting process. The two layer model for L1 and four layer model for L3 work well in both fitting, which illustrates the neutron scattering of Fe and N elements that accounts for the difference for each layer. It is also found out that the N concentration at the interface region is lower than that before annealing process.

PNR was conducted on these two samples, respectively, with field applied in-plane to saturate the magnetic moment. It is important to notice that these samples are different from the ones

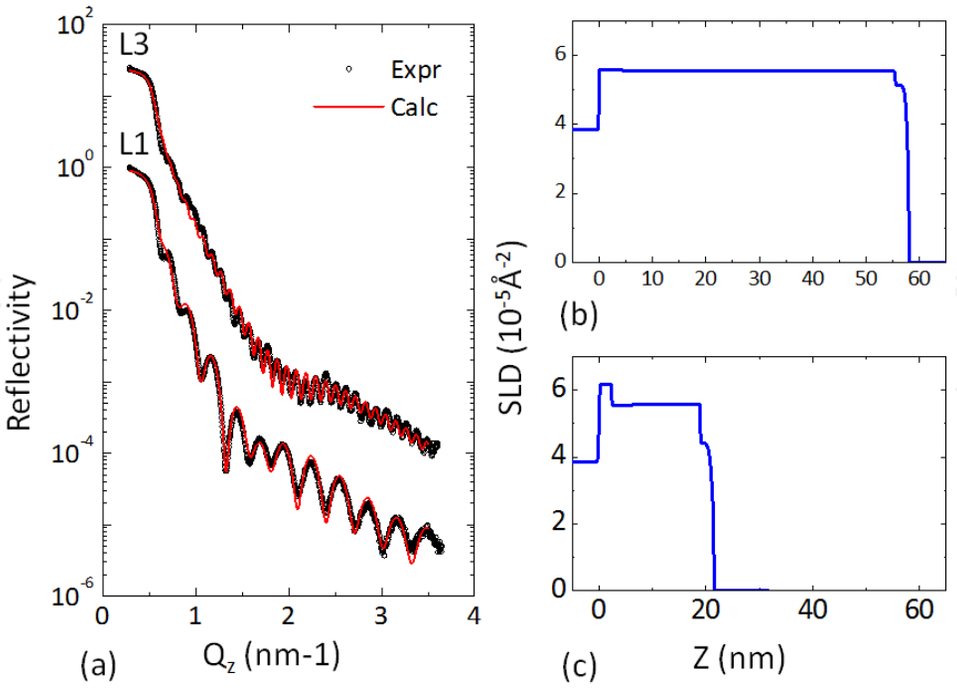

Figure 8. (a) X-ray reflectivity of $Fe_{16}N_2$ samples L1 and L3. (b) Electron SLD of L3 was homogeneous through the whole sample. (c) SLD of L1 stayed the same after the first ~2 nm bump.

with optimum FeN atomic ratio (Fe/N=8/1), whose Ms values are homogeneous throughout the film according to PNR measurement. In Fig. 9, reflectivity curves showed different oscillatory periods due to the differences in film thickness. Green lines of both samples in Fig. 9 (b) and (d) indicate the giant Ms at the bottom of the film, with a thickness of 5 nm, respectively. Since all the other FeN phases possess low Ms values, the only option for this enhancement should come from $Fe_{16}N_2$. Considering the fact that Fe seed layer is deposited before FeN layer, N atoms diffusion is most likely to occur to form $Fe_{16}N_2$ at the bottom as N atoms are initially rich on the top of Fe underlayer. $Fe_{16}N_2$ is formed at this specific location near the substrate with the right stoichiometric amount of N atoms. On the top of this giant Ms layer, a N rich phase is expected since N atoms are initially rich and a lower Ms result is obtained by PNR. This transition of Ms from high to low also occurs on L3. A reduced but still "giant" magnetization resides at the bottom interface. Compared to sample L1, the transition from high Ms to low Ms is comparably slow. Considering the XRD analysis achieved above, α"-$Fe_{16}N_2$ and α'-Fe-N martensites are present in the film structure. Since high Ms behavior is obtained, these observation on PNR analysis can only be explained by the presence of high Ms $Fe_{16}N_2$ phase and N rich phase. The formation of these mixture phases is most likely due to the strain that the film experiences with thinner Fe underlayer on the substrate. Multilayer structure of Fe/FeN provides the same environment of single Fe/FeN layer, but the difference is that higher Fe/FeN layers, which are not next to substrate, do not exhibit giant Ms. This is a result of the lattice strain relaxation in the film norm direction. To better demonstrate the fitting of PNR, chemical structure extracted from NSLD was checked and the corresponding model also fitted XRR data. It is noticeable that the bottom part of samples L1 and L3 have different

http://dx.doi.org/10.5772/62726

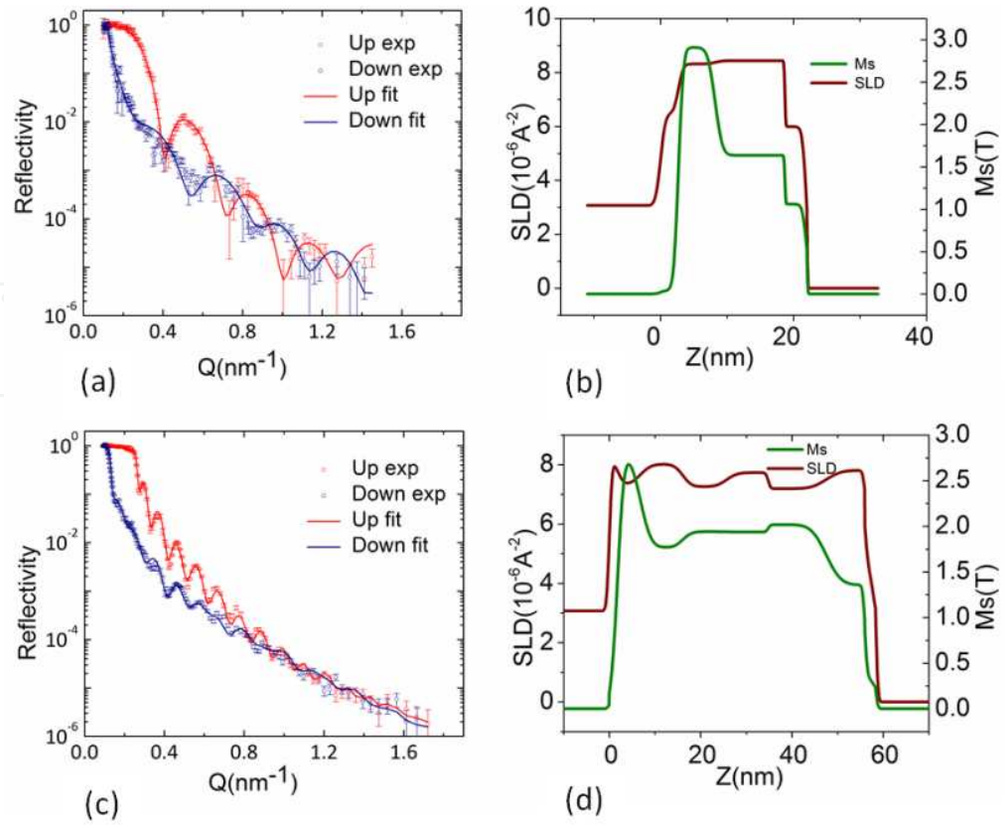

Figure 9. (a) Experimental and fitted reflectivity of sample L1. (b) Sample L1 SLD and Ms in-depth profile after fitting. (c) Experimental and fitted reflectivity of sample L3. (d) Sample L3 SLD and Ms in-depth profile after fitting. Both (b) and (d) curves exhibit high Ms value at bottom part of the film for ~5 nm scale.

electron and NSLD from XRR and PNR result. This region is most likely Fe and GaAs compound due to the inter-diffusion of Fe and GaAs atoms at their interface. The addition of this layer actually improved our fitting to the experiment data and was confirmed by SLD depth profile.

6. Using PNR to visualize the high perpendicular crystalline anisotropy [19]

The ordered $Fe_{16}N_2$ unit cell possesses tetragonality that gives rise to a high crystalline anisotropy, which is perpendicular to the film plane. This can be measured using vibrating sample magnetometer (VSM) in Fig. 10. However, VSM will not give detail information that will illustrate the FeN layer behavior in presence of the applied magnetic field.

During the PNR experiment, the external field is applied in the film plane direction. Both spin configuration signals are collected simultaneously. Fig. 11a–c show the reflectivity curves with fitting for spin-up and spin-down cases in three different external field intensities. At an external field of 20 kOe, the whole film magnetic moment will be saturated in the external field direction.

Since the same sample is tested in different fields, the chemical part, namely NSLD, stays the same during the fitting process. Three different MSLD depth profiles are generated after fitting in Fig. 11e. Since only one field intensity is strong enough to saturate the film in the film plane direction, the MSLD represent the in-plane component of the magnetization. It is clearly seen that the MSLD value drops rapidly for Fe-N layer, compared to Fe layer, when the external field is lowered. Since Fe layer is magnetically soft, all three fields will keep the Fe moment aligned in-plane. For Fe-N layer, there could be two scenarios to consider. First, the Fe-N film consists of antiferromagnetic domains in the film plane, which means the Fe-N layer has uniaxial in-plane anisotropy. This would directly contradict the fact that in-plane M-H loop does not depend on the in-plane orientation. Also, in this case, a strong off-specular signal should be observed, which is not our case either. Second, the magnetic moment turns out-of-plane due to perpendicular easy axis. This does explain our result since we do not observe off specular signal. When external field is lowered, the out-of-plane component of Fe-N film parallels the neutron beam momentum transfer and in-plane component contributes to the specular reflectivity. Therefore, the reduction of the magnetization in the in-plane direction after lowering external field can be explained by the out-of-plane easy axis of the Fe-N film.

Also, it is worth to mention that the oscillation amplitude of the reflectivity curves for R^- curve is much smaller than that of R^+ curve. This is most likely due to the modulation of the external field that the SLD is getting close to that of the substrate. This phenomenon is more robust when it approaches the Fe/GaAs interface where the reflectivity behavior is most dominated by this region at high q_z.

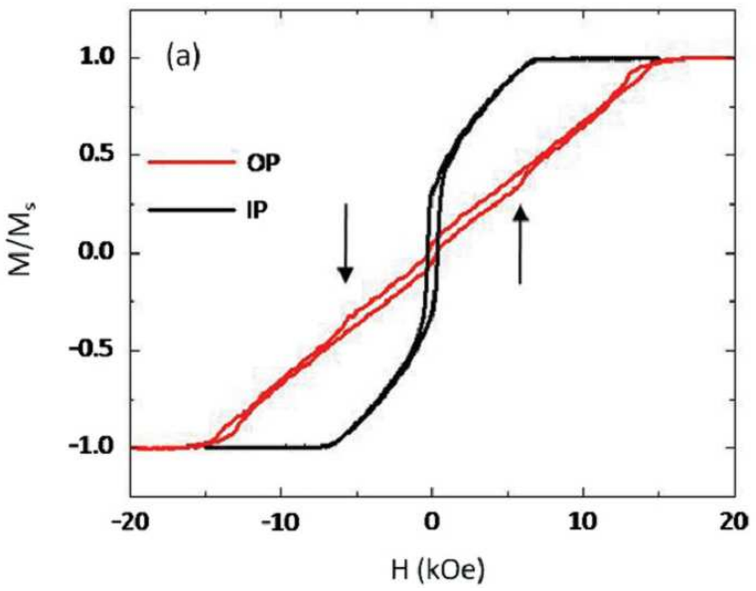

Figure 10. In-plane (black) and out-of-plane (red) M-H loops measured on one partially ordered $Fe_{16}N_2$ sample. The Fe-N layer switches at Hc~5.7 kOe (black arrows).

http://dx.doi.org/10.5772/62726

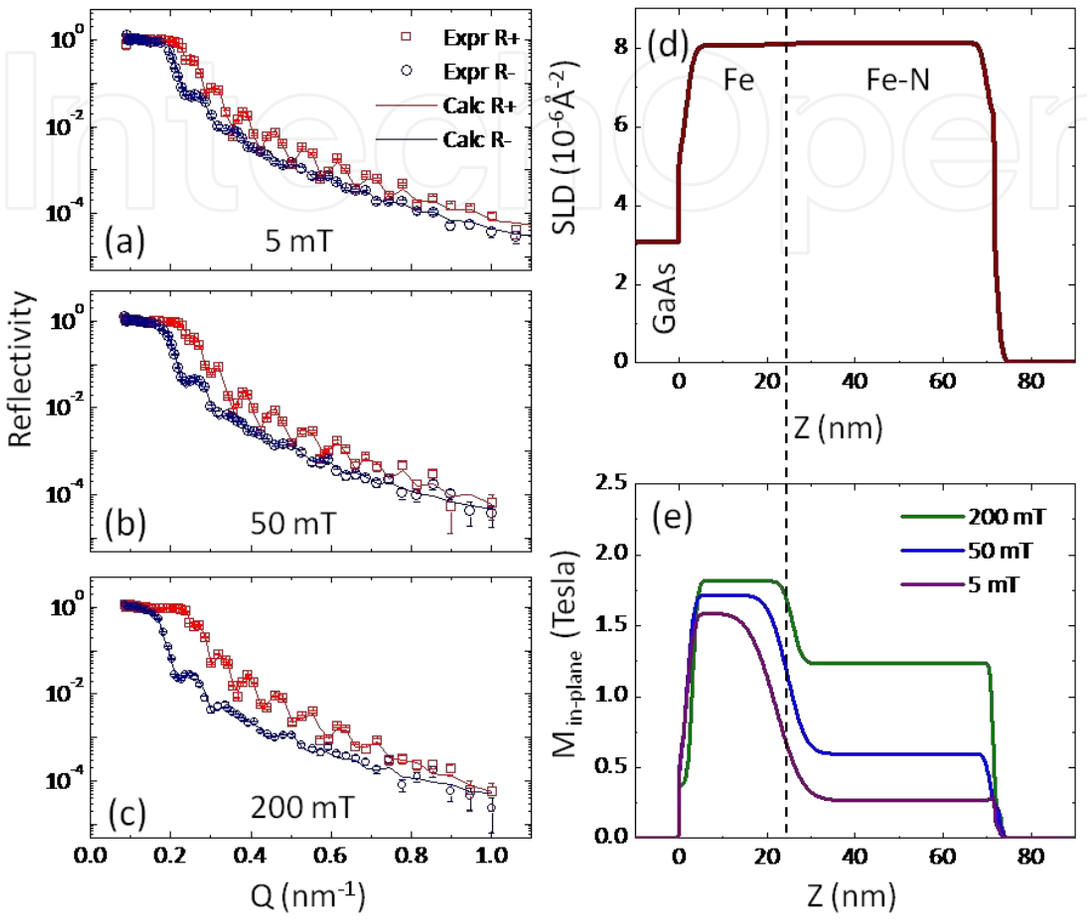

Figure 11. (a)–(c) Fitted reflectivity curves with experiment data of Fe-N sample at external field of 5, 50, and 200 mT, respectively. (d) NSLD depth profile of Fe-N sample and (e) MSLD, the in-plane magnetization component, depth profile of Fe-N sample at above three different external fields.

7. Summary

By using PNR, the Bs value can be accurately obtained directly in contrast to the conventional way that involves the thin film volume. In addition, we are also obtaining the Fe-N thin film NSLD and MSLD in-depth profile, which helps us to understand the physics behind the high Bs value. The above results are all derived from the specular reflections of the polarized neutron beam. This will facilitate the understanding of the giant Bs partially ordered $Fe_{16}N_2$ thin film in the film plane direction.

Acknowledgements

This work was partially supported by ARPA-E (Advanced Research Projects Agency- Energy) project under Contract No. 0472-1595, Seagate Technology and Western Digital. Parts of this work were carried out in the Characterization Facility through NSF MRSEC program at University of Minnesota.

Author details

Xiaowei Zhang[1,2*], Nian Ji[1,2], Valeria Lauter[3], Haile Ambaye[3] and Jian-Ping Wang[1,2]

*Address all correspondence to: jpwang@umn.edu

1 Electrical and Computer Engineering Department and the Center for Micromagnetics and Information Technologies (MINT), University of Minnesota, Minneapolis, Minnesota, USA

2 Physics Department, University of Minnesota, Minneapolis, Minnesota, USA

3 Neutron Science Scattering Division, Oak Ridge National Laboratory, Oak Ridge, Tennessee, USA

References

[1] T. K. Kim and Takahashi, Appl. Phys. Lett. 20, 492 (1972).

[2] Y. Sugita, H. Takahashi, M. Komuro, K. Mitsuoka and A. Sakuma, J. Appl. Phys. 76, 6637 (1994).

[3] M. A. Russac, C. V. Jahnes, E. Klokholm, J. Lee, M. E. Re, and B. C. Webb, J. Appl. Phys. 70, 6427 (1991).

[4] J.-P. Wang, N. Ji, X. Liu, Y. Xu, C. Sánchez-Hanke, Y. Wu, F. M. F. de Groot, L. F. Allard , and E. Lara-Curzio Depa.

[5] J. Chakhalian, J. W. Freeland, G. Srajer, J. Strempfer, G. Khaliullin, J. C. Cezar, T. Charlton, et al., Nat. Phys. 2, 4 (2006) 244–248.

[6] J. A. C. Bland, D. Pescia, and R. F. Willis, Phys. Rev. Lett. 58, 1244 (1987).

[7] M. A. M. Gijs, F. Petroff, Magnetic Ultra Thin Films, Multilayers and Surfaces Elsevier, 1997.

[8] J. A. C. Bland, J. Lee, S. Hope, G. Lauhoff, J. Penfold, D. Bucknall, J. Magn. Magn. Mater. 165, 46 (1997).

[9] S. J. Blundell, M. Gester, J. A. C. Bland, H. J. Lauter, V. V. Pasyuk, and A. V. Petrenko, Phys. Rev. B 51, 9395 (1995)

[10] J. A. Borchers, J. A. Dura, J. Unguris, D. Tulchinsky, M. H. Kelley, C. F. Majkrzak, S. Y. Hsu, R. Loloee, W. P. Pratt Jr., and J. Bass, Phys. Rev. Lett. 82, 2796 (1998).

[11] J. Hoppler, J. Stahn, C. Niedermayer, V. K. Malik, H. Bouyanfif, A. J. Drew, M. Rössle, A. Buzdin, G. Cristiani, H. U. Habermeier, and B. Keimer, Nat. Mater. 8, 315 (2009).

[12] X. L. Zhou and S. H. Chen, Phys. Rep. 257, 223–348 (1995).

[13] M. R. Fitzsimmons and C. F. Majkrzak, Application of Polarized Neutron Reflectometry to Studies of Artificially Structured Magnetic Materials. pp 15

[14] N. Ji, V. Lauter, X. Zhang, H. Ambaye, and J. P. Wang. Appl. Phys. Lett. 102, 072411 (2013).

[15] V. Lauter-Pasyuk, H.J. Lauter, B. Toperverg, O. Nikonov, E. Kravtsov, L. Romashev, V. Ustinov, J. Magn. Magn. Mater., 226 Part 2, 1694 (2001).

[16] V. Lauter, et. al., Physica B 404, 2543 (2009).

[17] http://wwwllb.cea.fr/prism/programs/simulreflec/simulreflec.html.

[18] X. Zhang, N. Ji, V. Lauter, H. Ambaye, and J. P. Wang, J. Appl. Phys. 113, 17E149 (2013).

[19] G. P. Felcher, Phys. Rev. B 24, 1595 (1981).

[20] C. F. Majkrzak, Physica B 173, 75 (1991).

[21] N. Ji, M. S. Osofsky, V. Lauter, L. F. Allard, X. Li, K. L. Jensen, H. Ambaye, E. Lara-Curzio and J.-P. Wang, Phys Rev B 84 (24), 245310 (2011).

IntechOpen